International Journal of Minerals, Metallurgy and Materials
Volume 26, Number 10, October 2019, Page 1217
https://doi.org/10.1007/s12613-019-1887-5

Investigating the mechanical and acoustic emission characteristics of brittle failure around a circular opening under uniaxial loading

Peng Li[1,2,3)], *Fen-hua Ren*[1,2,3)], *Mei-feng Cai*[1,2,3)], *Qi-feng Guo*[1,2,3)], *Hao-fei Wang*[1)], *and Kang Liu*[1)]

1) School of Civil and Resource Engineering, University of Science and Technology Beijing, Beijing 100083, China

2) Key Laboratory of High-Efficient Mining and Safety of Metal Mines (Ministry of Education of China), University of Science and Technology Beijing, Beijing 100083, China

3) Beijing Key Laboratory of Urban Underground Space Engineering, University of Science and Technology Beijing, Beijing 100083, China

(Received: 9 March 2019; revised: 2 July 2019; accepted: 8 July 2019)

Abstract: The size of underground openings in rock masses in metal mines is critical to the performance of the openings. In this study, the mechanical and acoustic emission (AE) characteristics of brittle rock-like specimens containing a circular opening with different ratios of opening diameter to sample size λ (λ = 0.1, 0.13, 0.17, 0.2, and 0.23) were investigated under uniaxial compression with AE monitoring. The results indicate that the opening size strongly affected the peak strength and the elastic modulus. Crack initiation first started from the upper surface of the specimens, not from the periphery of the openings. Tensile and shear cracks coexisted on the roof and floor of the specimens, whereas tensile cracks were dominant on the two sides. The fracture mode of samples with openings was partially affected by the relative size of the pillars and openings. The AE response curves (in terms of counts, cumulative energy, cumulative counts, and *b*-value) show that brittle failure was mainly a progressive process. Moreover, the AE information corresponded well with microcrack evolution in the samples and thus can be used to predict sample failure.

Keywords: rock mechanics; circular opening; opening size; uniaxial compression; acoustic emission

1. Introduction

The excavation and application of underground openings such as tunnels and vertical circular shafts in deep rock masses for metal mines are rapidly increasing worldwide. However, the construction of these underground openings may lead to stress concentration or release in the surrounding rock mass and may consequently cause local degradation or even overall degradation of the affected rock mass, decreasing its strength and increasing its hydraulic conductivity [1–2]. Meanwhile, the area around openings for which the rock mass state has changed significantly is usually accompanied by irreversible deformation, crack propagation, and the development of new cracks [3]; this affects the mechanical behavior of the rock mass over a broad area, thus affecting the long-term safety of the underground openings.

The stability of underground openings in metal mines has always been a critical issue, especially for high *in situ* stress conditions, which have a greatly increased probability of failure. To investigate the failure behaviors of underground openings, many studies have been carried out to examine rock or rock-like materials failure near openings through experiment or numerical simulation. For example, based on practical experience, Martini *et al.* [3] suggested that spalling appears in the area of maximum tangential stress around the boundary of an opening. Kratzsch [4] summarized four types of shaft deformation and failure patterns, i.e., the inclination of a central line, vertical compression or stretching, horizontal extrusion, and dislocation of the shaft wall. Fakhimi *et al.* [5] explored the loading failure behaviors around the underground excavation in a rock mass using a sandstone sample with a circular opening under biaxial loading condition. Gui *et al.* [6] numerically studied the influences of non-banded openings on the mechanical behaviors and fracture pattern of the rock mass and stated that the opening in the rock generally decreases the rock's strength and stiffness. Weng *et al.* [7] investigated the fracture evolution behavior around an opening under coupled

Corresponding author: Fen-hua Ren E-mail: renfh_2001@163.com

static-dynamic loading and concluded that the initial stress level remarkably affects the dynamic crack initiation stress, dynamic crack velocity, and failure mode of the samples. The previous works have contributed to understanding the failure characteristics and crack evolution in samples with an opening. However, the failure mechanism of underground openings is still incomplete. In addition to the effects of exogenous factors, many parameters of an opening itself—such as the opening size, distribution, and shape—can also affect the failure behaviors of the rock mass around the opening. For a specific opening shape, little attempt has been made to distinguish the differences in failure characteristics among specimens with different opening sizes. Practical experience indicates that the opening size inevitably influences the mechanical characteristics (such as compressive strength) and the crack propagation, coalescence, and failure modes near the opening in a brittle rock. Hence, determining a reasonable opening size is necessary in engineering practice.

In the present study, among the various opening configuration parameters, the opening diameter was the only chosen variable. The behaviors of the prepared brittle rock-like specimens with circular opening diameters of 15, 20, 25, 30, and 35 mm were investigated under uniaxial loading condition. Meanwhile, acoustic emission (AE) monitoring was conducted throughout the failure process for a detailed analysis. The mechanical strength and deformation, crack evolution and failure mode, and AE characteristics of the rock-like samples of interest were systematically analyzed. The research results can significantly enrich the understanding of brittle rock failure mechanisms and guide rock failure prediction, which can help prevent disasters at mine openings.

2. Experimental

2.1. Specimen preparation

Natural rocks generally have discontinuities, such as joints, fractures, and bedding planes, which may cause unpredictable interference in the uniaxial compression loading test results. Thus, numerous kinds of materials such as gypsum, cement, and cement-sand are widely used to produce rock-like specimens [2,8]. As a common laboratory test model material, cement has many advantages, such as its easy availability, low cost, and reproducibility; thus, it was selected as the rock-like material in this study to simulate rock masses with different diameter circular openings. The prepared synthetic rock-like specimens were made with high-early-strength cement and tap water in a proportion of 2:1 by weight. The sample preparation fabrication procedure was as follows: (1) the weighed mixture (i.e., the high-early-strength cement and tap water) was poured into a mechanical agitator and mixed at low speed for 3 min, and then mixed at high speed for 2 min to obtain a homogeneous cement paste. (2) The mixed cement slurry was poured into a carefully designed steel mold with a cylindrical steel shaft of known diameter to form an opening inside the sample. (3) The steel mold with the cement slurry was affixed to the vibration table and vibrated for approximately 1 min to exhaust the air bubbles inside the sample. (4) The paste was left to build up strength for approximately one hour, and then the specimen was carefully removed from the steel mold by dismantling it to ensure the specimen integrity. (5) The specimens were stored and cured in a standard curing box at a temperature of 20 ± 1°C and a humidity of approximately 95% for seven days before laboratory testing. The specimen preparation procedure is presented in Fig. 1. Note that the outer wall of the cylindrical steel shaft was coated with a lubricant (petroleum jelly) so that the sample can be easily separated from the steel shaft. The dimensions of the artificial rock-like specimens were 150 mm × 150 mm (height × width) with a thickness of 75 mm, and the circular opening diameters (D) inside the specimens were 15, 20, 25, 30, and 35 mm, as shown in Fig. 2. The ratio of opening diameters to the height or width of the entire model (λ) was approximately 0.1, 0.13, 0.17, 0.2, and 0.23, respectively. Compared with natural rocks, the rock-like samples exhibit more homogeneous and isotropic features because their particle size distribution is uniform and refined. The physical and mechanical properties (average values) for the intact rock-like samples are listed in Table 1. In terms of the strength parameters, the uniaxial compressive strength (UCS) of the intact sample is 30.18 MPa; the rock-like specimen can be considered as soft rock. Additionally, the ratio of the UCS to the uniaxial tensile strength exceeds 15, which indicates that the rock-like specimens exhibit significant brittleness [9].

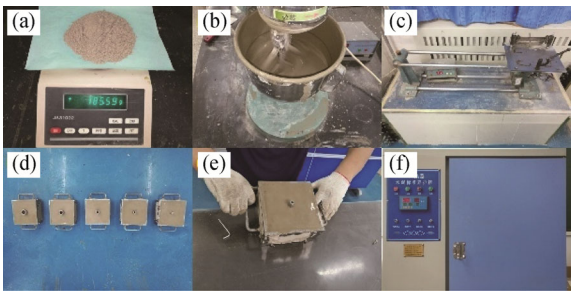

Fig. 1. Specimen preparation procedure: (a) weighing cement; (b) mixing and stirring; (c) vibration table; (d) standing for about an hour; (e) removing a specimen from a mold; (f) standard curing box.

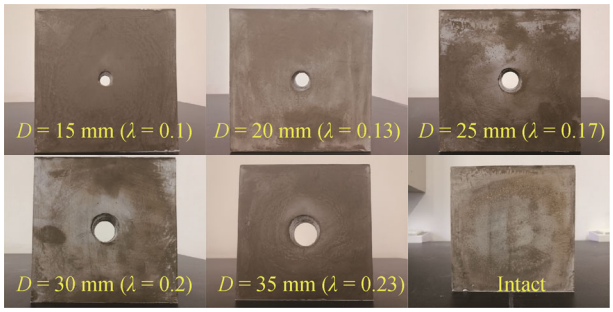

Fig. 2. Rock-like models with opening λ values of 0.1, 0.13, 0.17, 0.2, and 0.23, and an intact rock-like sample.

Table 1. Properties of the intact rock-like samples

Item	Experimental result
Density, ρ / (g·cm^{-3})	1.76
Uniaxial compressive strength, UCS / MPa	30.18
Uniaxial tensile strength, σ_t / MPa	1.96
Elastic modulus, E / GPa	0.76
Poisson's ratio, v	0.15

2.2. Test system

An RLW-3000 computer-controlled servo-hydraulic compression machine (Fig. 3(a)) was used for mechanical behavior testing. This machine contains a main loading structure with vertical and horizontal loading systems, which allows for uniaxial and biaxial loading tests. The maximum load capacity (vertical direction) of the machine is 3000 kN, and the axial load and displacements can be acquired automatically by the loading equipment. A six-channel AE monitoring system (PCI-2) (Fig. 3(b)) produced by Physical Acoustics Corporation (PAC), USA, was used to monitor the AE signals generated during specimen loading. The AE transducer (type R6α, from PAC) (Fig. 3(c)) is a resonant and highly sensitive instrument with a frequency response range of 0 to 300 kHz. The AE monitoring system has the advantages of a low threshold, fast processing speed, high reliability, and low noise, which effectively reduces the sampling noise. A schematic diagram showing the AE event waveform parameters is presented in Fig. 4, and detailed definitions of AE event terminology can be found in [10].

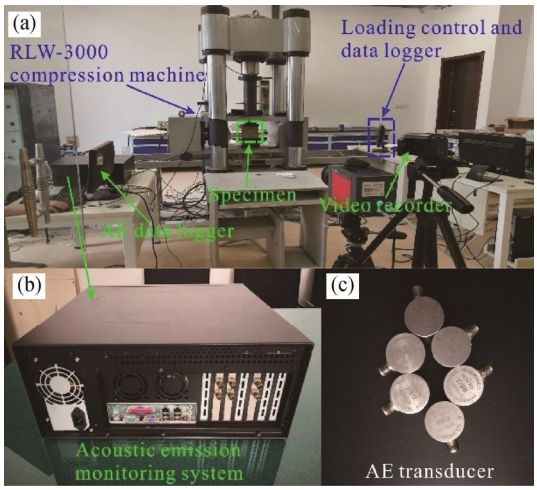

Fig. 3. RLW-3000 servo-controlled testing machine (a), PCI-2 AE monitoring system (b), and R6α AE transducers (c).

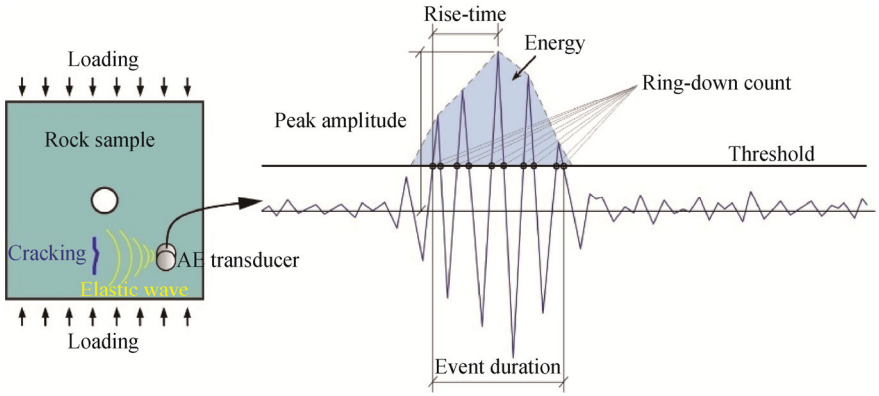

Fig. 4. Features of transient AE waveform generated from a loaded rock-like sample (modified as in Zhao *et al.* [11]).

2.3. Testing methods

Uniaxial loading was applied to the rock-like samples to study the rock mass behavior near openings with different λ values (Fig. 5(a)). The uniaxial loading test's experimental procedures involved the following steps: (1) Four AE transducers were arranged around the opening at four points approximately 30 mm away from the nearest specimen boundary (Fig. 5(b)) to better cover the specimen and precisely record the AE signals. The sensors surfaces were coated with a thin layer of petroleum jelly, and then the sensors were affixed to the specimen's surface with a rubber band to achieve good acoustic coupling between the sensors and the specimen and reduce AE signal attenuation. (2) The prepared sample was arranged on the test bench. The top and

bottom compressed planes of the specimen were coated with petroleum jelly to reduce the end friction between the sample and the loading platens during the test. (3) A 1 kN vertical load was pre-applied to ensure that the compressed planes of the specimen were in full contact with the loading platens and prevent the contact noise that is generated during contact from affecting the AE monitoring results. The vertical load was then gradually increased until the sample failed, and the AE signals were monitored continuously in real time. The entire experiment was monitored by a video recorder. Displacement-control mode was employed for the loading configuration, and the constant loading rate was set to be 0.1 mm/min to eliminate dynamic influences on the sample [2]. Note that in all tests, the compression machine and AE host were grounded to eliminate noise caused by the current. The AE signals transmitted from the four AE sensors were amplified with a gain of 40 dB to eliminate the influence of background noise. The trigger threshold magnitude of AE was set to 45 dB, and the full waveform data were automatically recorded at a 1 MHz data acquisition rate. Moreover, the timing of each test data acquisition system was synchronized before the tests to ensure that the data from the mechanical test and that of AE were strictly temporally matched.

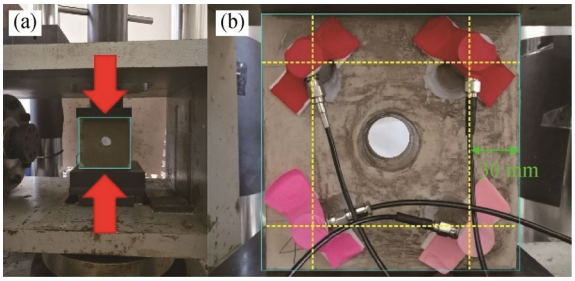

Fig. 5. Uniaxial loading configuration (a) and the designed positions of AE transducers on the specimen (b).

3. Results

3.1. Strength and deformation behavior of specimens

Fig. 6 shows the complete stress-strain curves of the uniaxial load test of the rock-like specimens. The specimens exhibited similar curve shapes, as expected, and experienced an initial compaction stage and a linear elastic deformation stage, and then the stress dropped sharply with the ringing sound of rupture, showing significant elastic-brittle failure, with a small amount of plastic deformation appearing near the peak strength. The stress–strain curves of the specimens in the uniaxial compression test (Fig. 6) agree well with the typical brittle behavior model, as illustrated in Fig. 7. It is worth noting that the curves in the initial compaction stage are slightly bent upward (Fig. 6), which may be a consequence of the compaction of a large number of microscopic/submicroscopic flaws/cracks, such as grain boundaries and internal and transgranular cracks in the specimens. Although the synthetic rock-like specimens are devoid of primary pores, they inevitably contain these microcracks, which are randomly distributed throughout the sample volume.

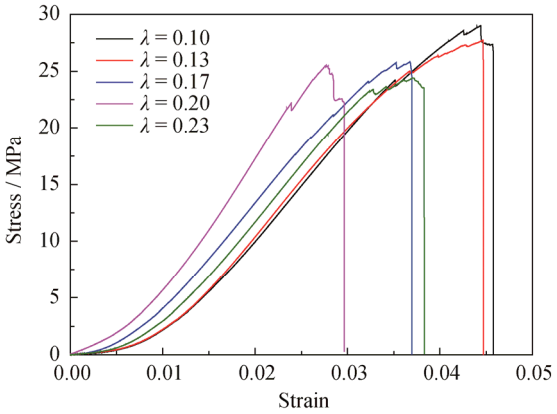

Fig. 6. Complete stress–strain curves for specimens with different opening sizes in the uniaxial compression test.

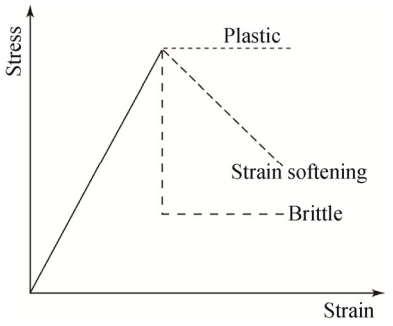

Fig. 7. Various post-peak responses used in continuum models [9].

Fig. 8 shows the experimentally obtained peak strength versus λ. The peak strength of the specimens decreased as λ increased from 0.1 to 0.23. The UCS of the intact specimen was 30.18 MPa (Table 1); the UCSs of specimens with λ = 0.1, 0.13, 0.17, 0.2, and 0.23 decreased by approximately 3.88%, 8.15%, 14.41%, 15.41%, and 19.12%, respectively. Hence, it can be deduced that the opening size had a significant influence on the specimen's strengths. Specifically, the changes in the UCS imply that the sample is more susceptible to cracking as the opening diameter increases. This is mainly due to the decrease in the relative size of the pillar, which aggravates the concentration of tensile stress around the opening, leading to early failure. Additionally, Fig. 8 il-

lustrates the change in the experimentally obtained elastic modulus (E) with λ to investigate the effect of λ on the elastic modulus. In the experimental results, E was calculated using the tangent modulus at the 1/2 failure stress level of the complete stress–strain curve. As depicted in Fig. 8, the E of the samples increased as λ increased from 0.1 to 0.2 and decreased as λ increased from 0.2 to 0.23, ranging generally between 0.59 and 0.78 GPa. The E of the intact specimen was 0.76 GPa (Table 1); the specimens with λ = 0.1, 0.13, 0.17, and 0.23 exhibited decreases in E of approximately 22.37%, 22.37%, 13.16%, and 21.05%, respectively, while the specimen with λ = 0.2 showed an increase of approximately 2.63%. Consequently, the effects of λ on the elastic modulus are remarkable. This result suggests that the opening size also plays a critical role in sample deformability. It should be noted that the trend in E is not consistent with the peak strength, and the samples with different λ values had high strength and low elastic modulus. Generally, elastic modulus and strength are different macroscopic manifestations of the mechanical properties of rock samples and are usually positively correlated. However, they have no definite mechanical relationship, and there are many exceptions, including negative correlation and noncorrelation [12–13]. This can be explained because a rock sample is an aggregate of mineral particles that are heterogeneous and anisotropic both microscopically and macroscopically; it is not an ideal linear elastomer. As mentioned earlier, the rock-like samples used were likely to contain microscopic/submicroscopic flaws/cracks, which may lead to the approximate negative correlation between elastic modulus and strength. This characteristic, however, still needs to be further studied.

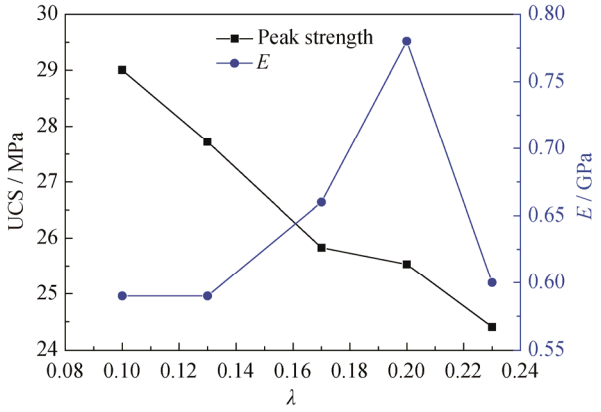

Fig. 8. Influences of opening diameter on the uniaxial compressive strength and the elastic modulus of the specimens.

3.2. Characteristics of failure mode and crack evolution

The failure behaviors of a rock mass with an opening are closely related to the stress distribution around the opening in the loaded condition. To better understand the failure mode and crack evolution of the tested specimens, the stress distribution characteristics around a circular hole needs to be briefly analyzed. Fig. 9(a) illustrates a circular cavity located in a homogeneous, isotropic, linear elastic, and non-creeping surrounding rock mass subjected to a vertical stress P and a horizontal stress kP (k is the lateral pressure coefficient). According to the elasticity theory, the stress distribution in the surrounding rock mass with a planar circular opening is given by [14]

$$\begin{cases} \sigma_r = \dfrac{1}{2}(1+k)P\left(1-\dfrac{R_0^2}{r^2}\right)-\dfrac{1}{2}(1-k)P\left(1-4\dfrac{R_0^2}{r^2}+3\dfrac{R_0^4}{r^4}\right)\cos 2\theta \\ \sigma_\theta = \dfrac{1}{2}(1+k)P\left(1+\dfrac{R_0^2}{r^2}\right)+\dfrac{1}{2}(1-k)P\left(1+3\dfrac{R_0^4}{r^4}\right)\cos 2\theta \\ \tau_{r\theta} = \dfrac{1}{2}(1-k)P\left(1+2\dfrac{R_0^2}{r^2}-3\dfrac{R_0^4}{r^4}\right)\sin 2\theta \end{cases} \tag{1}$$

where σ_r, σ_θ, and $\tau_{r\theta}$ are the radial stress, tangential stress, and shear stress, respectively, on the circumference at a distance r from the center of the circular opening in the polar coordinate system; R_0 is the radius of the circular hole; θ is the angle between the radius and the horizontal axis; P is the vertical stress; and k is the lateral pressure coefficient, which is equal to zero when the loading is uniaxial.

When $r = R_0$, Eq. (1) can be further simplified as

$$\begin{cases} \sigma_r = 0 \\ \sigma_\theta = P(1+k)-2P(1-k)\cos 2\theta \\ \tau_{r\theta} = 0 \end{cases} \tag{2}$$

In the uniaxial loading condition (k = 0), the tensile stress concentration coefficient at the roof and floor periphery of the opening is 1.0, and the compressive stress concentration coefficient at the periphery of the opening sidewall reaches 3.0. Accordingly, the tensile damage of the materials first appears, and the main tensile cracks will be theoretically formed at the roof and floor of the opening. A plot of the stress distribution law in an elastic rock mass around a circular opening subjected to uniaxial compressive load is presented in Fig. 9(b). It can be found that the maximum compressive stress is in the horizontal orientation, while the maximum tensile stress is parallel to the loading orientation, in other words, at the center of the roof and floor periphery of the opening. Therefore, tensile failure tends to appear in the center of the top and bottom of the opening, and the two sidewalls of the opening are prone to compressive failure. Note that although Eqs. (1) and (2) are suitable only for an opening located on an infinite plane, the excavation stress disturbance range of a circular opening is 3–5 times the

opening radius. If the smallest disturbance multiple, 3, is selected, the specimen sizes that are used can be considered to have little influence on the mechanical behavior of the rock mass near the opening. In addition, many other scholars have calculated the stress distribution around an opening of samples with similar sizes using Eqs. (1) and (2) [15–16].

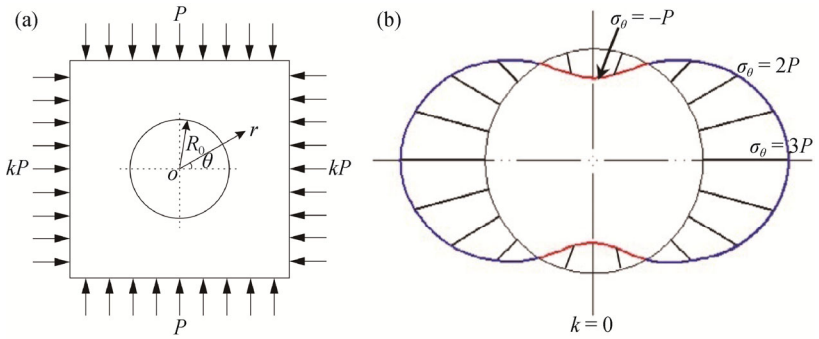

Fig. 9. A circular opening in an infinite medium (a) and the stress distributions around circular openings in homogeneous rock under uniaxial loading (b) [14].

Detailed views of the ultimate fracture behavior of the rock-like samples with λ equal to 0.1, 0.13, and 0.2 under uniaxial loading are shown in Figs. 10(a), 10(b), and 10(d). The two samples with λ equal to 0.17 and 0.23 burst suddenly during uniaxial loading (see the schematic diagrams in Figs. 10(c) and 10(e)), which may be due to the brittleness of the samples. Therefore, only the failure mode and crack evolution characteristics of the samples with λ equal to 0.1, 0.13, and 0.2 were analyzed. Video recorder monitoring results revealed that the sample failures were locally progressive. Crack initiation first started from the upper surface on all the specimens, rather than at the peripheries of the openings. The cracks then gradually propagated to the holes, primarily toward points in the horizontal radial direction of the holes. Moreover, the developed cracks grew parallel to the loading direction. Specifically, as shown in Figs. 10(a), 10(b), and 10(d), the λ values were 0.1, 0.13, and 0.2; initial cracks (generally tensile cracks) were first found at the top of the circular openings, and then shear cracks appeared near the openings and almost penetrated through the entire sample. Tensile and shear cracks coexisted on the roof and floor of the specimens. Tensile cracks were dominant on the two sides, whereas shear cracks generally penetrated through the openings or the areas near the opening. The microcracks on the left and right of the openings apparently tended to further grow toward their original directions. When the loading stresses reached the peak strengths of the samples, crack zones on both sides penetrated the entire specimens and formed macroscopic cracks (Figs. 10(a), 10(b), and 10(d)). This observation aligns with the theoretical analysis (Fig. 9(b)).

Although the forms of the crucial primary cracks causing specimen failure in Figs. 10(a), 10(b), and 10(d) are generally the same, some differences still exist in the obtained macroscopic overall failure modes among these three samples with different opening sizes. Specifically, the failure mode of the specimen with λ = 0.1 shows splitting along multiple planes (including shear failure along the opening) (Fig. 10(a)); the specimen with λ = 0.13 shows partial shear near the opening and spalling (Fig. 10(b)); and the specimen with λ = 0.2 shows shear failure along the opening and partial spalling (Fig. 10(d)). These differences may be because the fracture mode of a sample with precut openings is partially affected by the relative size of the pillars and openings. However, all three failure modes obtained in this study demonstrate that extension cracks occur at the top or the bottom of the openings and spalling or slabbing appears on the sidewalls, which agrees with existing conclusions [7]. This may be because the redistributed stress around the openings produces lateral stress at the roof and the floor of the openings. Moreover, the failure modes generally coincide with the sample fracture results of brittle granites obtained by Xu *et al.* [15]. In summary, the above analysis not only illustrates the correctness of the failure modes around the opening obtained in this study but also shows that it is suitable to use rock-like samples to simulate the failure of a natural brittle rock with an opening.

Observations of the tested brittle sample failures suggest that the brittle failure process involves the initiation, growth, and coalescence of microcracks. Microcrack initiation is mainly due to stress concentrations at the microscopic/submicroscopic flaw or crack ends in the samples. Notably, only microcracks with proper directions and dimensions will create new microcracks at their tips. In addition, the crack coalescence process can be considered a function of the distribution and interrelationship of the preexisting mi-

croscopic cracks [17]. This view is supported or supplemented by various failure modes of the rock-like samples under uniaxial compression in this study (Fig. 10). During uniaxial loading, the crack initiation begins at the preexisting microcrack tips in the samples and then reaches the stage of stable crack growth, which is followed by unstable crack propagation starting below the crack-damage stress. The unstable crack propagation ultimately results in sample failure. Moreover, the density, distribution, and mode of the microcracks during the stable and unstable crack propagation stages are quite different from the properties of the preexisting microcracks [17]. The crack locations formed around the openings during loading are basically aligned with the orientation of the maximum principal stress (here, the vertical direction). The direction of the macroscopic crack is nearly the same as that of the maximum principal stress.

Additionally, with increased opening diameter, the width of the final formed crack tends to increase (Fig. 10). The opening may function as a stress concentrator as the specimen is subjected to uniaxial compression. As the opening diameter enlarges, the stress concentration location will typically be easy to fracture. Hence, corresponding support measures should be taken during the construction of large underground circular cavities to prevent collapse.

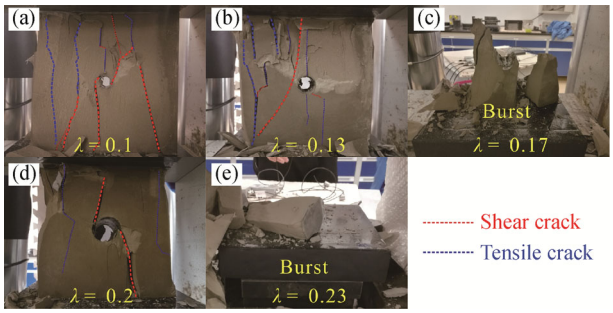

Fig. 10. Ultimate fracture behaviors of rock mode with different λ values during uniaxial loading: (a) λ = 0.1; (b) λ = 0.13; (c) λ = 0.17; (d) λ = 0.2; (e) λ = 0.23.

3.3. Acoustic emission characteristics of specimens

During the early phase of specimen loading, the initial microscopic/submicroscopic flaws or cracks in the specimens are compacted and closed, causing an AE phenomenon. The continuously increasing load will cause drastic changes in the stress around the opening, and numerous AE events will occur, along with the formation of considerable microcracks in the specimen when the sample stress reaches a certain level. As a phenomenon that accompanies the sample failure process, AE contains much information about the sample's internal deformation characteristics and mechanical behavior [18–19]. The AE information can directly reflect the evolution of microcracks in samples and can also be used to capture the precursors of sample failure. Many parameters (such as AE absolute energy, waveforms, counts, hits, rise time, duration, and derived *b*-value) have been used to characterize the AE characteristics of a rock mass [20]. In this paper, AE counts, cumulative energy, cumulative counts, and *b*-value are employed to reflect the AE behaviors of the tested samples during loading. Notably, for each specimen, four sensors were placed to record the AE signals. However, to ensure the AE signals can be effectively and continuously recorded during sample fracture, of the four sensors, only the sensor with the best and most comprehensive AE data and that best matches the stress–strain curves was selected to calculate the AE parameters [21–23].

Fig. 11 shows the evolution characteristics of the AE counts accompanied by the corresponding stress–time–count curves during uniaxial loading. It can be seen that the change trends of the AE counts of the samples with the five opening diameters (i.e., λ = 0.1, 0.13, 0.17, 0.2, and 0.23) are highly similar. Generally, the AE events accumulated throughout the uniaxial test of rock-like specimens in this study show a noticeable "stage" characteristic over the entire test process and can be classified into four main stages: the loading stage, the pre-event stage, the random event stage, and the coalesced fracture stage. The loading stage applies to the portion of the specimen testing with limited AE events, which are caused by the initial microscopic/submicroscopic flaw or crack closure and friction in the compaction process. The pre-event stage is the loading span during which no appreciable AE events occur in the sample when it is loaded below its strength. The random event stage signifies the beginning of appreciable AE event occurrence. During the random event stage, AE events are typically distributed randomly throughout the specimen. The AE events in this stage signify the material reacting to a loading condition that causes micro-fractures throughout the sample. The randomized nature of the events in this stage reflects the load finding the weak or stress-concentrated regions in the specimen. The coalesced fracture stage occurs when randomized events begin to coalesce into a predictable macro fracture direction; this stage continues until the fracture of the main sample. The typical fracture stage classification in the AE events versus loading plot can be seen in Fig. 11. On the other hand, the final AE count values for the λ = 0.13 and 0.17 specimens are approximately equal and are slightly greater than those of the other three specimens. Additionally, the five AE response curves in Fig. 11 show that the AE drop in the coalesced fracture stage is not apparent in brittle

failure. The rock-like specimens failed immediately after the AE peak, which corresponds to the stress change characteristics. Consequently, the AE peak can be regarded as an indication for the failure of the brittle specimens.

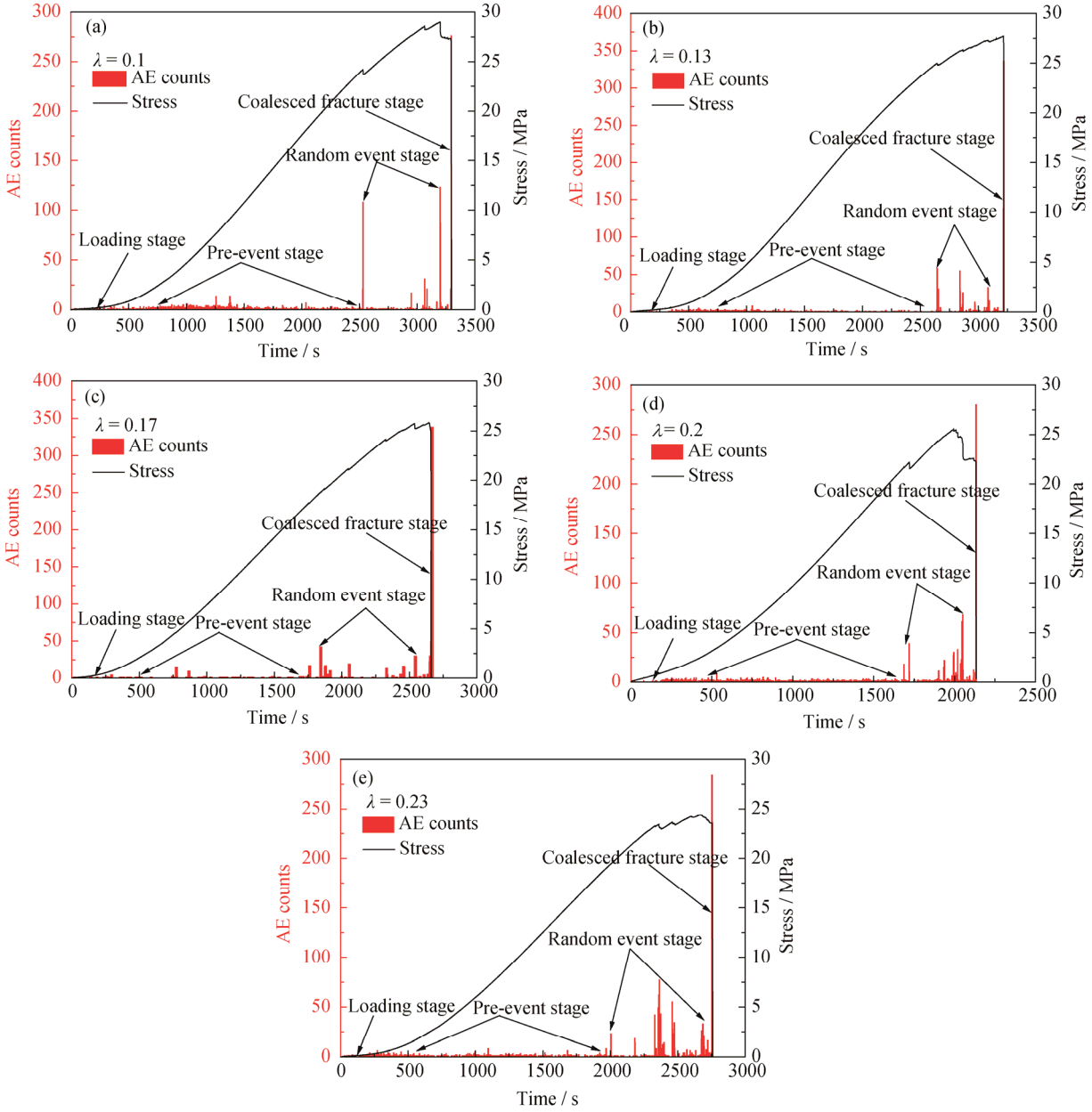

Fig. 11. Stress–time–count curves for rock-like specimens in the uniaxial test: (a) $\lambda = 0.1$; (b) $\lambda = 0.13$; (c) $\lambda = 0.17$; (d) $\lambda = 0.2$; (e) $\lambda = 0.23$.

Fig. 12 illustrates the cumulative energy and count–time curves for the unconfined load test on the rock-like specimens. For the specimens with λ value from 0.1 to 0.23, the AE evolution laws in terms of cumulative energy during stress loading are similar and generally have three stages: (1) During the initial stage, the cumulative energy of AE is close to zero, and the curves are approximately horizontal straight lines. (2) In the steady increase stage, the cumulative energy gradually increases in a step shape. (3) In the sudden increase stage, the cumulative energy increases sharply in a very short time, and the curves rise steeply. This result validates the accelerated release of AE energy before the failure. On the other hand, the cumulative count curves for samples with different opening sizes have similar general trends and all feature slow increase and sudden increase processes (Fig. 12). However, the cumulative count curves also show significant differences in the slow increase stage. The differences may not only be caused by the differences in the opening diameters of the samples, which also probably reflects the fact that a single consistent AE response

curve does not exist but that there are diverse AE response curves [21]. Based on the AE cumulative count curves under uniaxial compression obtained in this study (Fig. 12), four typical cumulative count curves are summarized in Fig. 13(a). The labels on each AE curve are numbered "1" through "4"; a region of linear elastic deformation, labeled "2" on each curve, was present in all four signatures. These signatures and descriptions are of great help for viewing the AE response curves of each specimen for which data were obtained. The AE cumulative counts cover all important processes that occur in the specimens from the initial application of the load to the complete failure. Theoretical considerations and AE cumulative counts can give us insight into the mechanism of specimen fracture in compression. Therefore, an interesting generalized observation is made on the typical AE cumulative count curves versus the imposed stress level of the specimens analyzed, as presented in Fig. 13(b), which can be correlated with the heuristic concepts of the brittle rock fracture process given by Bieniawski [24]. The labels "1" through "4" on the AE curve correspond with the regions identified in Fig. 13(a). As noted in Fig. 13(b), the process of fracture growth in the rock-like specimen is mainly characterized by two stages: stable and unstable fracture growth.

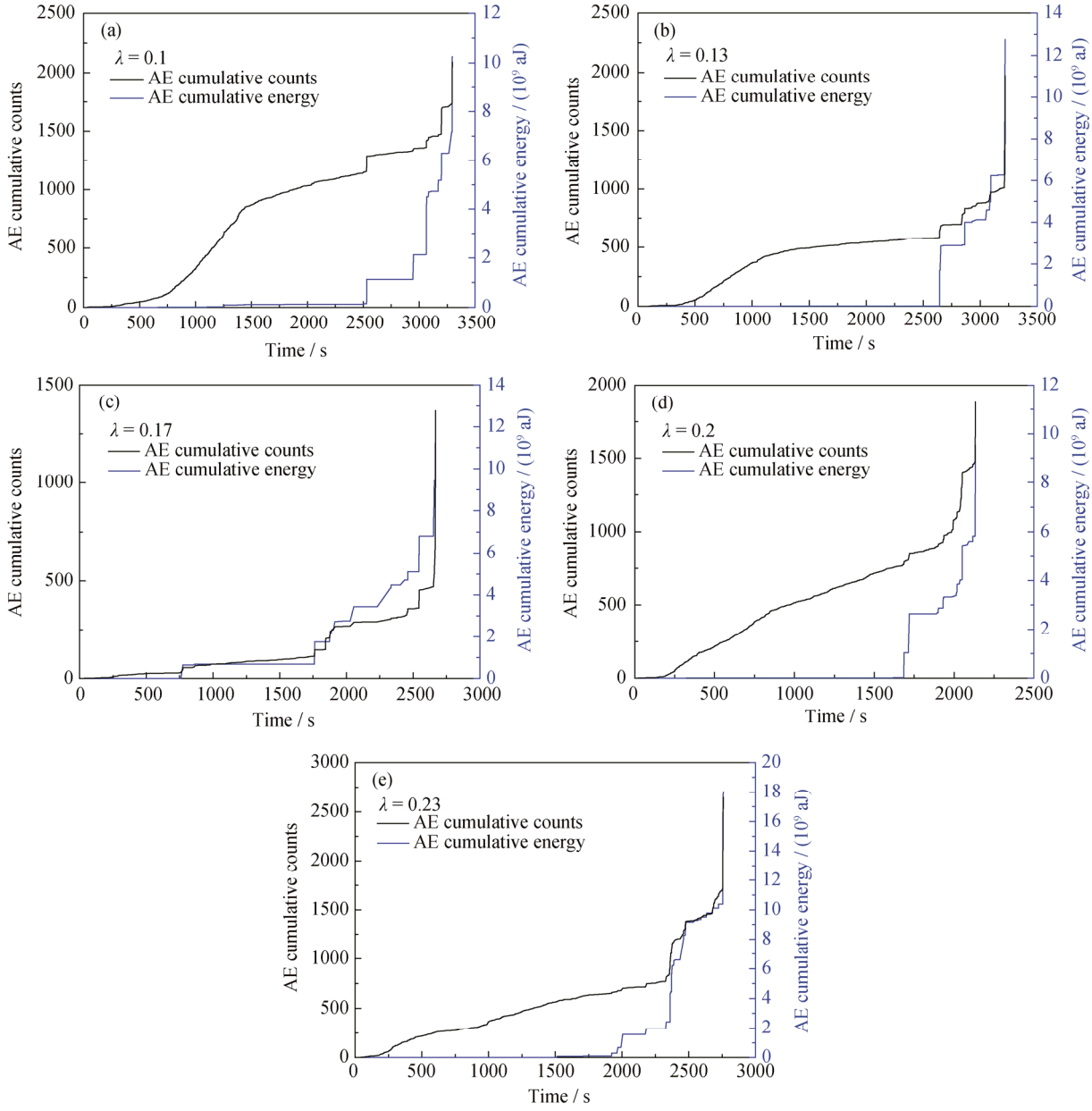

Fig. 12. Cumulative energy and count–time curves for the uniaxial test of rock-like specimens: (a) $\lambda = 0.1$; (b) $\lambda = 0.13$; (c) $\lambda = 0.17$; (d) $\lambda = 0.2$; (e) $\lambda = 0.23$.

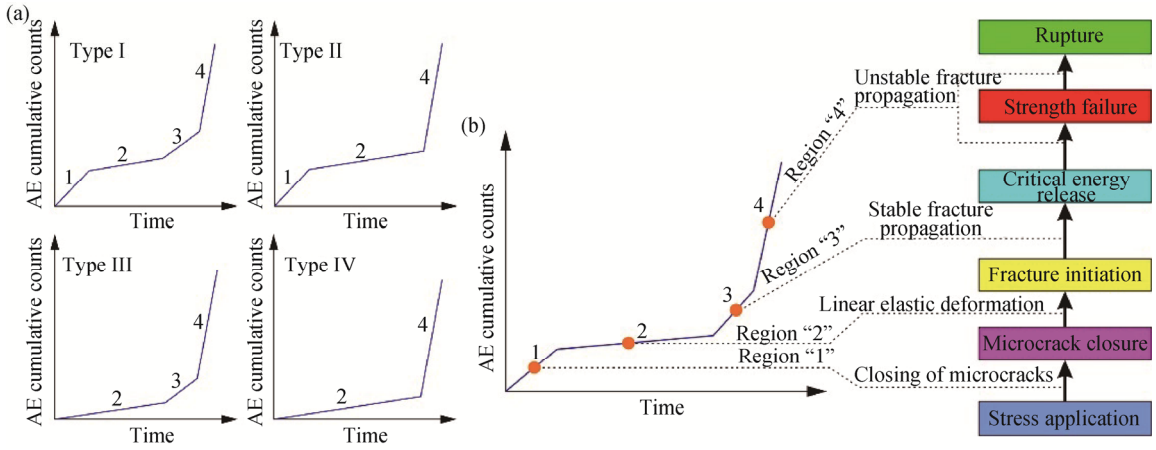

Fig. 13. Four types of AE signatures found for rock-like specimens under uniaxial loading (a) and the AE signature and its connection to the brittle fracture process (b) (modified as in Meyer [21]).

The *b*-value analysis (i.e., magnitude-frequency distribution analysis) can provide an additional means to characterize specimens with different λ values. The original relationship determined by Gutenberg and Richter [22] was adapted to correlate the annual number (average frequency) of earthquakes with corresponding earthquake magnitudes. To date, this relationship has been widely used to investigate rock failure, especially the propagation and evolution processes of rock cracks, in geotechnical and rock mechanics applications [22,25–26].

The relationship between the magnitude and frequency can be expressed as

$$\log_{10}(N) = a - bM \tag{3}$$

where M is the earthquake magnitude; N is the number of earthquake events that lie within $M \pm \Delta M$, which is considered as the number of AE events of samples in this study; and a and b are empirical constants.

Eq. (3) shows that the constant b represents the slope of the magnitude-frequency distribution plot. For rock AE, the *b*-value represents a function of the crack propagation scale [26]. The basic concept is that as the rock damage becomes more localized, the *b*-value decreases. Previous studies suggest that the *b*-value drops to a value far less than approximately 1.0 when samples become unstable, such as during the generation of macrocracks in samples [24]. Moreover, the *b*-value is closely related to the size of the AE sample space, the AE N value, and the determination of magnitude M. Commonly, the AE energy presented on a logarithmic scale can replace the earthquake magnitude M. The magnitude step spacing was selected to be 0.5, i.e., $\Delta M = 0.5$, and the N value is the count by the cumulative frequency. According to the AE test acquisition frequency, to prevent the calculation error of the *b*-value from being too large due to a too-small calculation interval, 100 AE events are taken as sliding windows and the initial time of the windows is taken as the time for calculating the *b*-value, and the AE event frequency N and the average energy value M representing magnitude in each window are obtained, and thus, the corresponding *b*-value is obtained. The *b*-values are calculated using an in-house developed MATLAB code. This yields *b*-values in the same range as those seen in seismic applications.

Fig. 14 illustrates the change trends of the *b*-values with time in the entire failure process for specimens with various λ values. It can be observed that the variation characteristics of the sample *b*-values are basically the same under uniaxial loading conditions and all show an evolution pattern of fluctuation in the first half of loading, followed by rapid decline before failure. Specifically, from the start of loading to approximately 90% of the peak stress, the *b*-values of the samples fluctuate within a certain range (generally between 0.1 and 0.5) and show an overall downward trend, which reflects the gradual development of microcracks. The fluctuation of the *b*-values also indicates the stress adjustment inside the samples due to crack propagation, but the samples still maintain their structural integrity during this process. The physical meaning of the *b*-value is a measure of crack development and evolution [26]. In other words, the overall magnitudes and change trends of the *b*-value are closely related to the development of cracks in the samples. As shown in Fig. 14, when the *b*-value decreases in a phase, it indicates that the proportion of small AE events decreases and the number of large AE events increases. When the *b*-value increases in a phase, it means that the number of small AE events increases. When the *b*-value changes steadily with a small amplitude in a phase, it implies that the number of

occurrences of large and small AE events is roughly equal and stable (such as Fig. 14(c)), and the crack growth of the sample is gradual and stable under this condition. Remarkably, each large drop occurs after a phase of gradual increase in *b*-value, as shown in Fig. 14; that is, small cracks first occur and then a large one occurs, implying coalescence of the just-formed cracks. In addition, the *b*-values of the samples drop sharply when the corresponding stresses drop before failure. After that, the *b*-values drop rapidly and reach their lowest points at the main point of rupture. Combined with the stress–strain curve, it is believed that a sudden change in the *b*-value corresponds to a stress drop in the samples and brittle failure of the samples. Near the peak stress, the small cracks coalesce and develop into large macrocracks. At this time, the number of large-energy events increases. An abrupt decrease in the *b*-value indicates a change in the development form of cracks in samples, and cracks propagate dramatically, which is a sign of an increase in AE events, and the samples may be damaged. The physical mechanism of the decrease in *b*-value before sample failure can be attributed to two aspects [27]: the microcracks in the sample change from tensile fracture to shear fracture,

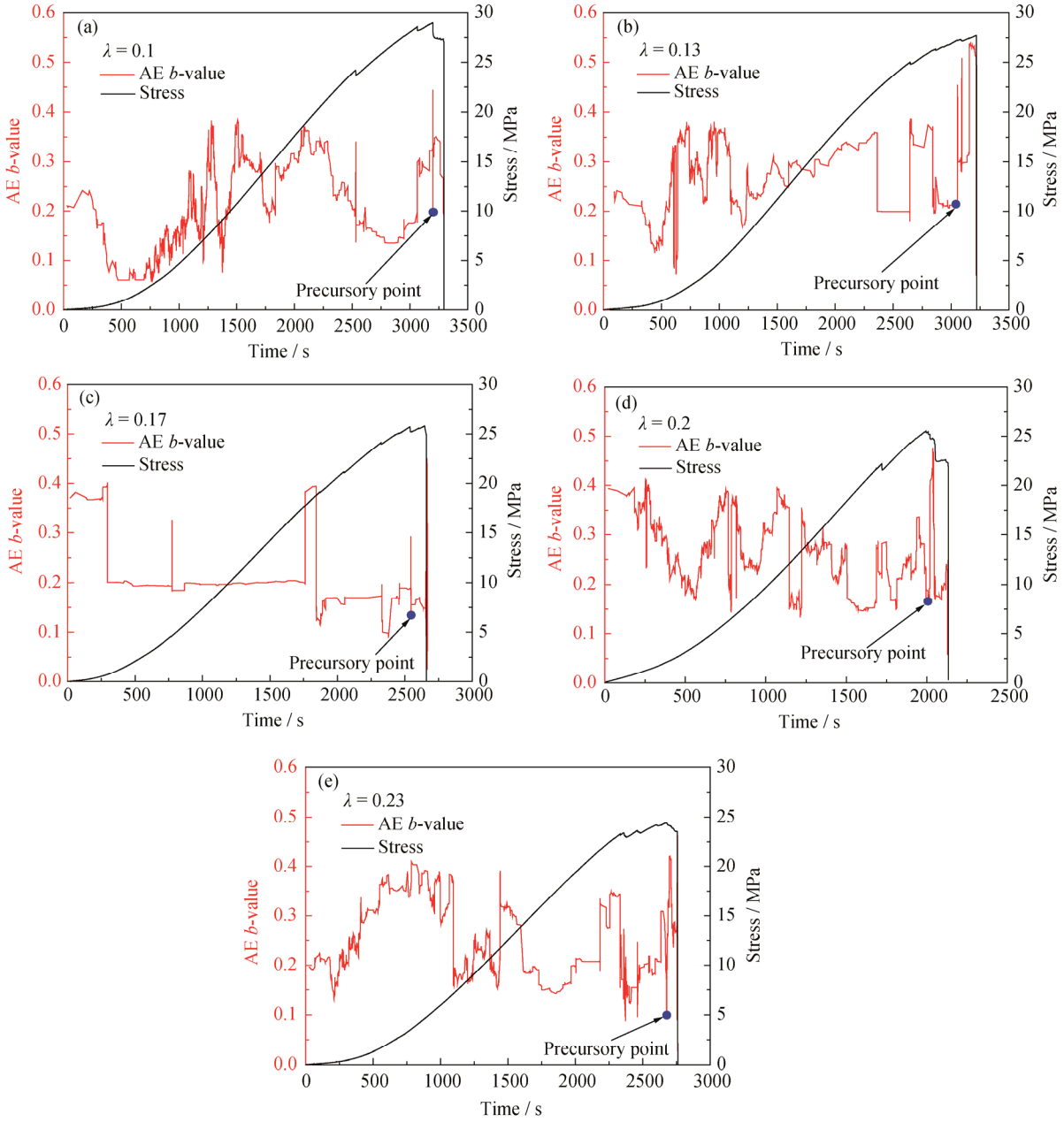

Fig. 14. Variation of *b*-values with time for test samples with different λ values: (a) $\lambda = 0.1$; (b) $\lambda = 0.13$; (c) $\lambda = 0.17$; (d) $\lambda = 0.2$; (e) $\lambda = 0.23$.

and secondly, the crack interaction is highly enhanced. The combined effect of these two aspects significantly increases the number of large events and decreases the *b*-value. The minimum point on the *b*-value curve of a sample is close to the curve's final decline stage, when the AE feature is extremely active. This point can be regarded as the precursor point of the sample failure. The precursor points of the samples with different λ values are marked in Fig. 14. The stress values corresponding to the precursor points of the samples with λ = 0.1, 0.13, 0.17, 0.2, and 0.23 are approximately 91.28%, 90.26%, 94.70%, 90.09%, and 94.51% of their own peak stresses, respectively. This result can be applied to predict damage at underground openings.

4. Discussion

As noted, the peak strength of all rock-like samples containing a single circular hole used in this paper is less than 30 MPa, which is much lower than that of real hard rocks (such as sandstone and marble). However, the experimental results obtained in this paper are comparable. For example, Li *et al.* [16] studied the deformation and fracturing process of marble samples with a single circular or elliptical hole using digital image correlation. They found that for samples with holes of different geometric shapes, the fracture develops from primary tensile fractures to secondary fractures and then to shear fractures. The two tensile cracks first initiate from the top and bottom of the existing openings and propagate along the loading direction. With the initiation and propagation of secondary cracks on the left and right sides of the openings, the two tensile cracks gradually close, and the tensile strain concentration areas disappear. Finally, the diagonal high-strain zones intersect at the left and right sides of the openings, resulting in the final macroscopic failure of the samples. Crack coalescence behavior around elliptical and circular openings in sandstone specimens was investigated by Huang *et al.* [28] using photographic and AE monitoring; they found that the tensile cracks appeared at the upper and lower parts of the samples, while shear stress concentration occurred on the sidewalls of the hole. With increasing load, more tensile damage appeared at the top and bottom of the hole. However, shear failure patterns were only captured at the two sides of the hole. Moreover, cracks originating from the perimeter surfaces of the oval or circular holes were considered to be shear cracks, tensile cracks, and composite shear and tensile cracks. In summary, the above test results further validate the inferences in this study, that is, those of the composite tensile and shear cracks shown in Fig. 10.

The fracture behaviors of a brittle sample with an opening are closely correlated with the scale, particle size, and discontinuity of the sample. A visual inspection of the samples tested in this study indicates that the designed sample diameters are more than 20 times larger than that of the rock, meeting the recommendations by the International Society for Rock Mechanics (ISRM) [7]. Moreover, the opening sizes are much greater than the particle size, and the experimental results from samples with different opening diameters prepared under the same conditions follow an acceptable trend. As mentioned previously, the height and width of the tested specimens were each 150 mm, and the thickness was 75 mm. Thus, the aspect ratio of the samples is equal to 1.0, which is considered small compared to the ISRM test criterion, which suggests an aspect ratio of 2.5–3.0 for uniaxial compression loads. For a brittle sample with a small aspect ratio (< 1.0), the fractures at areas far from the opening are typically caused by tensile failure, because large sections of the sample may be subjected to greater confinement due to the friction between the specimen and the platens [29–30]. Similarly, Hajiabdolmajid *et al.* [9] pointed out that brittle failure mainly results from the growth and coalescence of tensile cracks, and that tensile crack generation precedes shear failure, based on the theoretical analysis. This conclusion is also strongly supported by the results obtained in the present study (Fig. 10). Conversely, the failure mode of brittle samples that have a large aspect ratio (> 1.0) appears to be shear failure [31]. However, these conclusions still need to be validated by the real failure mode of underground openings in mining engineering.

To achieve our goal, the prepared rock-like samples can be regarded as isotropic rock masses, which eliminates the interference of other factors on the opening failure behavior. In mining engineering practice, the rock mass around the underground openings usually shows anisotropy due to preexisting and/or mining-induced discontinuities, such as joints and faults. The existence of such discontinuities alters the peripheral stress distribution pattern around the underground openings in terms of orientation and magnitude, which may lead to various rock mass failure modes, such as spalling, slabbing, and V-shaped notches, around the openings [2]. Consequently, the real fracture behaviors of mining engineering rock masses around underground openings may not be completely consistent with those of the homogeneous isotropic rock-like samples tested in the laboratory. However, Weng *et al.* [7] stated that the influence of the discontinuities is not remarkable and results similar to those in laboratory tests can be obtained under the condition of relatively high *in situ* stress in the natural brittle rock mass. Therefore,

further studies are still necessary to investigate the degree of influence of discontinuities with different scales and occurrence on the failure modes around the brittle rock mass openings.

Additionally, during the excavation and service of underground openings in metal mines, vault displacement is generally used as an important monitoring parameter to assess the stability of the openings. The displacement monitored at the top can be used as an early warning signal for the failure of rock masses with small and large openings. The failure mode and the time required for the failure of openings with different sizes vary. The experimental results in this study show that with the increased opening size, the sample failure time tends to decrease (Figs. 11 and 14). As Sagong *et al.* [2] explained, in a rock mass with a large opening, the fracture of the rock mass is likely to be disastrous and unexpected. Similarly, in this study, the samples with λ values of 0.17 and 0.23 suddenly burst during loading. This may be coincidental, but it also warns us that for rock masses with large opening sizes, special care is required even with a small rock mass displacement. However, the displacement caused by rock fracture can be expected to be more gradual with a small opening size and a stable rock mass. The observations obtained here show that different *in situ* opening stability monitoring standards in metal mines should be formulated and used for rock masses with different opening sizes.

5. Conclusions

(1) The prepared rock-like samples exhibited significant brittleness. The peak strength of the specimens decreased as the ratio of the opening diameters to the model's height or width, λ, increased from 0.1 to 0.23. The opening size strongly affected the peak strength and the elastic modulus of the samples. Larger diameter openings and smaller relative pillar sizes can aggravate the tensile stress concentration degree around the opening, leading to earlier failure. Moreover, the opening size appears to play a critical role with respect to the samples deformability.

(2) In the uniaxial compression test, the failures of all tested samples were locally progressive. Crack initiation first started on the upper surface of the specimens, not from the periphery of the openings. Tensile and shear cracks coexisted on the roof and floor of the specimens. Tensile cracks were dominant on the two sides, whereas shear cracks generally penetrated through the openings or in the area near the opening. The fracture mode of the samples with an opening was partially affected by the relative size of the pillars and openings. The prepared cement samples effectively simulated the failure of a brittle rock with an opening.

(3) The AE information effectively reflected the evolution of microcracks in the samples and thus can be used as an additional predictor of sample failure. The change trend of the AE counts of the samples with different opening diameters are highly similar and can be classified into four main stages: the loading stage, the pre-event stage, the random event stage, and the coalesced fracture stage. The AE peak can be regarded as an indication of the failure of brittle specimens. The AE cumulative energy curves of all tested samples generally had three stages: an initial stage, a steady increase stage, and a sudden increase stage, demonstrating the accelerated release of AE energy before sample failure. The cumulative count curves of the samples with the five opening diameters showed significant differences in the slow increase stage. From the start of loading to approximately 90% of the peak stress, the *b*-values of all tested samples fluctuated within a certain range (generally between 0.1 and 0.5) and exhibited an overall downward trend, which reflects the gradual development of the microcracks.

Acknowledgements

This work was financially supported by the National Natural Science Foundation of China (No. 51774022), the State Key Research Development Program of China (No. 2016YFC0600801), the Beijing Natural Science Foundation (No. 2184108), and the China Postdoctoral Science Foundation (No. 2017M620620). Dr. Masoud RahJoo at the University of British Columbia is greatly acknowledged for his constructive advice and review of this article.

References

[1] R. Pusch and R. Stanfors, The zone of disturbance around blasted tunnels at depth, *Int. J. Rock Mech. Min. Sci. Geomech. Abstr.*, 29(1992), No. 5, p. 447.

[2] M. Sagong, D. Park, J. Yoo, and J.S. Lee, Experimental and numerical analyses of an opening in a jointed rock mass under biaxial compression, *Int. J. Rock Mech. Min. Sci.*, 48(2011), No. 7, p. 1055.

[3] C.D. Martini, R.S. Read, and J.B. Martino, Observations of brittle failure around a circular test tunnel, *Int. J. Rock Mech. Min. Sci.*, 34(1997), No. 7, p. 1065.

[4] H. Kratzsch, *Mining Subsidence Engineering*, Springer, Berlin, 1983, p. 92.

[5] A. Fakhimi, F. Carvalho, T. Ishida, and J.F. Labuz, Simulation of failure around a circular opening in rock, *Int. J. Rock Mech. Min. Sci.*, 39(2002), No. 4, p. 507.

[6] Y.L. Gui, Z.Y. Zhao, C. Zhang, and S.Q. Ma, Numerical in-

vestigation of the opening effect on the mechanical behaviours in rocks under uniaxial loading using hybrid continuum-discrete element method, *Comput. Geotech.*, 90(2017), p. 55.

[7] L. Weng, X.B. Li, A. Taheri, Q.H. Wu, and X.F. Xie, Fracture evolution around a cavity in brittle rock under uniaxial compression and coupled static–dynamic loads, *Rock Mech. Rock Eng.*, 51(2018), No. 2, p. 531.

[8] R.H. Cao, P. Cao, H. Lin, G.W. Ma, X. Fan, and X.G. Xiong, Mechanical behavior of an opening in a jointed rock-like specimen under uniaxial loading: Experimental studies and particle mechanics approach, *Arch. Civ. Mech. Eng.*, 18(2018), No. 1, p. 198.

[9] V. Hajiabdolmajid, P.K. Kaiser, and C.D. Martin, Modelling brittle failure of rock, *Int. J. Rock Mech. Min. Sci.*, 39(2002), No. 6, p. 731.

[10] E. Eberhardt, D. Stead, B. Stimpson, and R.S. Read, Identifying crack initiation and propagation thresholds in brittle rock, *Can. Geotech. J.*, 35(1998), No. 2, p. 222.

[11] X.G. Zhao, M. Cai, J. Wang, and L.K. Ma, Damage stress and acoustic emission characteristics of the Beishan granite, *Int. J. Rock Mech. Min. Sci.*, 64(2013), p. 258.

[12] M.Q. You, C.D. Su, and X.S. Li, Study on relation between mechanical properties and longitudinal wave velocities for damaged rock samples, *Chin. J. Rock Mech. Eng.*, 27(2008), No. 3, p. 458.

[13] Q.H. Wu, M.Q. You, and C.D. Su, Mechanical parameters and their relativity of anisotropy granite, *J. Cent. South Univ. Sci. Technol.*, 46(2015), No. 6, p. 2216.

[14] H.Q. Zhang, H. Shi, H.W. Jing, Y. Wu, and H. Pu, Numerical study of remote fracturing around a circular opening in rock, *Eur. J. Environ. Civ. Eng.*, 2018.

[15] S.D. Xu, Y.H. Li, and J.P. Liu, Detection of cracking and damage mechanisms in brittle granites by moment tensor analysis of acoustic emission signals, *Acoust. Phys.*, 63(2017), No. 3, p. 359.

[16] D.Y. Li, Q.Q. Zhu, Z.L. Zhou, X.B. Li, and P.G. Ranjith, Fracture analysis of marble specimens with a hole under uniaxial compression by digital image correlation, *Eng. Fract. Mech.*, 183(2017), p. 109.

[17] A. Basu and D.A. Mishra, A method for estimating crack-initiation stress of rock materials by porosity, *J. Geol. Soc. India*, 84(2014), No. 4, p. 397.

[18] X.P. Lai, L.H. Wang, and M.F. Cai, Couple analyzing the acoustic emission characters from hard composite rock fracture, *J. Univ. Sci. Technol. Beijing*, 11(2004), No. 2, p. 97.

[19] J.L. Pei, W.P. Fei, and J.F. Liu, Spatial evolution and fractal characteristics of natural fractures in marbles under uniaxial compression loading based on the source location technology of acoustic emission, *Environ. Earth Sci.*, 75(2016), No. 9, p. 828.

[20] X. Wang, Z.J. Wen, Y.J. Jiang, and H. Huang, Experimental study on mechanical and acoustic emission characteristics of rock-like material under non-uniformly distributed loads, *Rock Mech. Rock Eng.*, 51(2018), No. 3, p. 729.

[21] B.J. Meyer, *New Objective Method for the Determination of Crack Initiation Stress Using Acoustic Emission Data, A* [Dissertation], Colorado School of Mines, Golden, 2018, p. 23.

[22] T. Schumacher, *New Acoustic Emission Applications in Civil Engineering* [Dissertation], Oregon State University, Corvallis, 2010, p. 22.

[23] Q.Q. Zhu, D.Y. Li, Z.Y. Han, X.B. Li, and Z.L. Zhou, Mechanical properties and fracture evolution of sandstone specimens containing different inclusions under uniaxial compression, *Int. J. Rock Mech. Min. Sci.*, 115 (2019), p. 33.

[24] Z.T. Bieniawski, Stability concept of brittle fracture propagation in rock, *Eng. Geol.*, 2(1967), No. 3, p. 149.

[25] M.V.M.S. Rao and K.J.P. Lakshmi, Analysis of *b*-value and improved *b*-value of acoustic emissions accompanying rock fracture, *Curr. Sci.*, 89(2005), No. 9, p. 1577.

[26] L.M. Zhang, S.Q. Ma, M.Y. Ren, S.Q. Jiang, Z.Q. Wang, and J.L. Wang, Acoustic emission frequency and *b* value characteristics in rock failure process under various confining pressures, *Chin. J. Rock Mech. Eng.*, 34(2015), No. 10, p. 2057.

[27] X.L. Lei, K. Kusunose, M.V.M.S. Rao, O. Nishizawa, and T. Satoh, Quasi-static fault growth and cracking in homogeneous brittle rock under triaxial compression using acoustic emission monitoring, *J. Geophys. Res. Solid Earth*, 105(2000), No. B3, p. 6127.

[28] Y.H. Huang, S.Q. Yang, M.R. Hall, W.L. Tian, and P.F. Yin, Experimental study on uniaxial mechanical properties and crack propagation in sandstone containing a single oval cavity, *Arch. Civ. Mech. Eng.*, 18(2018), No. 4, p. 1359.

[29] B.J. Carter, E.Z. Lajtai, and A. Petukhov, Primary and remote fracture around underground cavities, *Int. J. Numer. Anal. Methods Geomech.*, 15(1991), No. 1, p. 21.

[30] H. Munoz and A. Taheri, Specimen aspect ratio and progressive field strain development of sandstone under uniaxial compression by three-dimensional digital image correlation, *J. Rock Mech. Geotech. Eng.*, 9(2017), No. 4, p. 599.

[31] H. Güneyli and T. Rüşen, Effect of length-to-diameter ratio on the unconfined compressive strength of cohesive soil specimens, *Bull. Eng. Geol. Environ.*, 75(2016), No. 2, p. 793.